Research Square

Preprints are preliminary reports that have not undergone peer review.
They should not be considered conclusive, used to inform clinical practice,
or referenced by the media as validated information.

Phosphorylation of IRS4 at YY111/112 promotes LUSC progression via PI3K/AKT pathway activation

Jian Huang

jyhuanj@shsmu.edu.cn

Shanghai Jiao Tong University School of Medicine https://orcid.org/0000-0002-5033-9622

Yilixiati Aihemaiti

Qiuhan Ren

Xiangling Jiang

Kaideya Wushaying

Ran Chen

Shanghai Jiaotong University School of Medicine

Yanli Wang

Xian Zhao

Department of Biochemistry and Molecular Cell Biology, Shanghai Key Laboratory of Tumor Microenvironment and Inflammation, Shanghai Jiao Tong University School of Medicine

Lei Xu

Zhi Yang

Jianxiu Yu

Shanghai Jiao Tong University School of Medicine https://orcid.org/0000-0002-6515-6001

Article

Keywords: IRS4, Tyrosine phosphorylation, Src, PI3K-AKT, LUSC

Posted Date: May 20th, 2026

DOI: https://doi.org/10.21203/rs.3.rs-9421260/v1

License: This work is licensed under a Creative Commons Attribution 4.0 International License.
Read Full License

Additional Declarations: There is **NO** conflict of interest to disclose.

Version of Record: A version of this preprint was published at Oncogene on October 17th, 2026. See the published version at https://doi.org/10.1038/s41388-026-04015-0.

Abstract

Lung squamous cell carcinoma (LUSC) lacks effective targeted therapies despite frequent hyperactivation of the PI3K/AKT pathway, and the contribution of adaptor proteins to this process remains poorly defined. Here, we identify Insulin Receptor Substrate 4 (IRS4) as a common substrate of Src kinase and the phosphatase RPTPα, and uncover a previously unrecognized, conserved phosphorylation site at YY111/112 within the IRS4 PH domain. Src-mediated phosphorylation at this site is essential for IRS4-driven proliferation, anchorage-independent growth, and invasiveness in LUSC cells. Mechanistically, phosphorylation at YY111/112 induces conformational rearrangements in IRS4 that enhance the recruitment of the p85β SH2 domain to the YXXM motif of IRS4, thereby promoting AKT activation without altering IRS4 protein stability or subcellular distribution. An IRS4-derived cell-permeable phosphopeptide containing pYY111/112 disrupts the Src–IRS4 interaction and significantly suppresses tumor growth in vivo in a YY111/112-dependent manner. Consistently, YY111/112 phosphorylation is markedly elevated in human LUSC tissues and correlates with advanced disease stages. Collectively, these findings define a Src–IRS4–PI3K/AKT signaling axis and identify YY111/112 as a critical regulatory site of IRS4 and a potential therapeutic vulnerability in LUSC

INTRODUCTION

Lung cancer remains the most significant cause of cancer-related mortality worldwide, with lung squamous cell carcinoma (LUSC) accounting for approximately 30% of all cases[1]. While lung adenocarcinoma has seen a transformation in clinical management through the targeting of specific mutations in EGFR or ALK, LUSC is characterized by a high mutational burden and a notable lack of validated therapeutic targets[2, 3]. Comprehensive proteogenomic characterizations have consistently identified hyperactivation of the PI3K/AKT/mTOR signaling pathway as a feature of LUSC[4, 5]. Previous studies in this field have largely focused on the oncogenic roles of kinases, emphasizing how their overexpression or hyperactivation drives malignant transformation[6, 7]. In contrast, the contribution of docking adaptor proteins to tumor development has received comparatively limited attention. Pan-cancer analysis of somatic copy number alterations and chromatin structure revealed that the rearrangement of the cis-regulatory factor mediated the upregulation of IRS4 expression, particularly in LUSC[8, 9].

The insulin receptor substrate (IRS) family of proteins is a group of essential adapter proteins that link cell-surface receptors to intracellular signaling cascades[10]. This family comprises IRS1, IRS2, IRS3, and IRS4, all of which share similar structural domains, including the N-terminal Pleckstrin homology (PH) domain, the phosphotyrosine-binding (PTB) domain, and the C-terminal docking site[11]. IRS1 and IRS2 are the two most-studied proteins, widely expressed across various human tissues. IRS3 is a pseudogene in the human genome, whereas IRS4 is mainly expressed in limited tissues, including the kidney, ovary, liver, and thymus[12]. Unlike IRS1 and IRS2, the IRS4 protein lacks the SHP2 binding motif that provides negative feedback regulation, making it relatively insensitive to signal attenuation [13]. This structural divergence allows IRS4 to sustain signaling activity for longer durations once activated [14].

Multiple studies have confirmed that the overexpression of IRS4 is significantly associated with aggressive clinical features and poor prognosis across various malignancies[15]. Non-receptor tyrosine kinase Brk has been identified as a key kinase that phosphorylates the IRS4 protein in breast cancer [16]. Similarly, in ovarian cancer, the tyrosine kinase FER phosphorylates IRS4 to activate the PI3K-AKT signaling axis, thereby facilitating malignant cell proliferation[17]. In hepatocellular carcinoma, IL-4 stimulation promotes IRS4 phosphorylation and induces malignant progression[18]. IRS4 is constitutively membrane localized and recruits PI3K, SHP-2, and PKC upon phosphorylation without requiring protein translocation in rat hepatocytes[19]. IRS4 is essential for IGF-I-stimulated growth by activating p70S6K and a non-canonical, Ras-independent ERK signaling pathway in HepG2 cells[20]. PILRB recruits the deubiquitinase OTUB1 to stabilize the IRS4 scaffold, preventing its proteasomal degradation and sustaining PI3K/AKT hyperactivation in gastric cancer[21].

IRS4 is an intracellular adaptor protein that mediates signal transduction from tyrosine kinases to downstream pathways governing cell growth and survival[15]. Increasing evidence indicates that aberrant IRS4 activation contributes to tumorigenesis by enhancing PI3K and AKT signaling, thereby promoting cancer cell proliferation and survival [22]. Despite these findings, the biological role of IRS4 and the mechanisms regulating its activity in lung squamous cell carcinoma remain poorly defined. Src is a non-receptor tyrosine kinase that plays a central role in tumor initiation and progression by regulating proliferation, survival, migration, and invasion[23, 24]. Elevated Src activity is frequently observed in lung cancer and is associated with tumor invasiveness and poor clinical prognosis[25, 26]. Receptor-type protein tyrosine phosphatase alpha (RPTPα) is a well-established positive regulator of Src signaling, activating Src by dephosphorylating Tyr527[27, 28]. RPTPα has also been implicated in tumorigenesis, although the downstream substrates through which it modulates oncogenic signaling remain incompletely characterized [29].

In this study, we identify IRS4 as a common substrate of the tyrosine kinase Src and the phosphatase RPTPα, and uncover a previously unrecognized phosphorylation site at Tyr111 and Tyr112. We show that phosphorylation at these residues promotes a conformational change in IRS4 that enhances recruitment of the PI3K regulatory subunit p85β, thereby augmenting activation of the PI3K–AKT signaling pathway. Importantly, phosphoproteomic analysis of LUSC patient samples reveals elevated phosphorylation of IRS4 at Tyr111/112 in tumors, which positively correlates with disease progression, highlighting the clinical relevance of this regulatory mechanism.

RESULTS

IRS4, which is associated with clinical progression, interacts with both Src and RPTPα

Building on our long-standing interest in the RPTPα-Src signaling pathway, we analyzed our previous mass spectrometry (MS) datasets to explore new regulatory components of this oncogenic network[29]. By intersecting the RPTPα interactome driven from our MS analysis with predicted Src and RPTPα

binding partners from the GeneCards database, only three proteins met the screening criteria (Fig. 1A). Among them, Grb2 is a known binding partner of RPTPα, which further validates the reliability of our mass spectrometry data. The CANX gene encodes the chaperone protein calnexin, which is primarily involved in endoplasmic reticulum protein folding and is currently not relevant to our research focus. However, IRS4 is known to play an important role in cellular signal transduction and has also been found to be aberrantly expressed in certain cancers. To evaluate the clinical relevance of IRS4, we analyzed its expression levels across a wide range of cancer types. The results revealed that *IRS4* mRNA expression significantly and positively correlates with advanced clinical stages, with a progressive increase from Stage 0 to Stage IV (Fig. 1B). These data suggest that IRS4 may play a critical role in tumor progression across multiple cancer types. Therefore, IRS4 was selected as the target molecule for our subsequent studies.

Given the bioinformatic prediction, we experimentally validated the physical interaction between IRS4 and the non-receptor tyrosine kinase Src. Exogenous co-immunoprecipitation (Co-IP) analysis in 293T cells showed IRS4 can interact with Src (Fig. 1C). This interaction was further confirmed under physiological conditions via endogenous Co-IP analysis (Fig. 1D). Additionally, GST pull-down analysis demonstrated that purified GST-Src effectively captured Myc-IRS4, indicating a direct and stable association (Fig. 1E). Further, to map which domain of Src is involved in the interaction with IRS4. A series of GST-tagged Src truncation mutants was constructed based on its modular structure, including ΔSH1, ΔSH2, ΔSH3, and ΔSH4 (Fig. S1A). GST pull-down assays were performed by incubating these recombinant GST-Src variants with cell lysates expressing Flag-tagged full-length IRS4. As shown in Fig. S1B, the interaction between Src and IRS4 was significantly abolished upon the deletion of the SH3 domain. Next, we sought to identify the reciprocal binding interface on IRS4. We generated three truncated IRS4 fragments corresponding to its functional domains: the PH domain, the PTB domain, and the C-terminal domain, as indicated (Fig. S1C). These His-tagged fragments were purified and subjected to GST pull-down assays with recombinant GST-Src. Our data revealed that the PH domain of IRS4 exhibited the strongest binding signal to Src, whereas the PTB or C-terminal domains showed a relatively weaker interaction (Fig. S1D). Collectively, these findings demonstrate that Src physically associates with IRS4 primarily through a specific interaction between its SH3 domain and the PH domain of IRS4.

To confirm if IRS4 is a bona fide substrate of RPTPα, we employed a "substrate-trapping" strategy. This method involves mutating invariant residues in the PTP catalytic domain to create a mutant enzyme that retains high affinity for substrates but is catalytically impaired, thus "trapping" the enzyme-substrate complex[30]. In our analysis, we utilized the RPTPα phosphatase-inactive mutant (CC433/723SS) for this trapping mechanism[31]. Co-IP analysis in 293T cells revealed that Myc-RPTPα-CC433/723SS mutant exhibits more high affinity to Flag-IRS4 compared with RPTPα WT as expected (Fig. 1F). The endogenous association between native RPTPα and IRS4 was also confirmed in 293T cells by Co-IP analysis (Fig. 1G). Finally, GST pull-down analysis further validated that purified GST-RPTPα, both WT and CC/SS mutant could directly pull down Flag-IRS4; moreover, Myc-RPTPα-CC433/723SS mutant exhibits more high affinity to Flag-IRS4 (Fig. 1H). These findings establish that IRS4 acts as a substrate for both Src

and RPTPα, potentially modulating the phosphorylation-dependent signaling events mediated by these two enzymes.

Phosphosite analysis of IRS4 by Src kinase

To elucidate the regulatory mechanisms governing IRS4 activity, we first characterized its tyrosine phosphorylation in response to Src signaling. In 293T cells, co-expression of Myc-IRS4 with either wild-type Src or the constitutively active mutant (Y530F) induced a robust increase in IRS4 tyrosine phosphorylation (Fig. 2A). This phosphorylation was markedly abrogated by the Src-specific inhibitor, Saracatinib or by the kinase-inactive Src mutant (Y419F). Furthermore, we observed that RPTPα dose-dependently reduced IRS4 phosphorylation induced by activated Src (Fig. 2B). Together, these results indicate that IRS4 tyrosine phosphorylation is tightly controlled by opposing actions of Src and RPTPα, suggesting that IRS4 activity is regulated through a balanced interplay between phosphorylation and dephosphorylation.

To pinpoint the specific residues targeted by Src kinase, we performed an *in vitro* kinase (IVK) assay coupled with mass spectrometry (MS). Due to the large molecular weight of the IRS4 protein (160 kDa), we were unable to express the full-length protein in a prokaryotic system. Consequently, we purified various His-tagged IRS4 truncations (PH, PTB, and C-terminal domain) along with GST-Src to perform IVK experiments (Fig. 2C). Immunoblot analysis showed that the C-terminal domain of IRS4 was the main region of phosphorylation. The PH and PTB domains also showed some phosphorylation modification (Fig. 2D). Subsequent mass spectrometry analysis of phosphorylated IRS4 fragments identified a total of 11 tyrosine phosphorylation sites (Fig. 2E-F, S2A). Notably, among these residues, Y112 was identified for the first time in our MS analysis, representing a novel phosphorylation event on IRS4. While the other ten tyrosine phosphorylation sites are **consistent with those reported on the** PhosphoSite database[32]**.**

Notably, since five phosphorylation sites have already been studied in a previous study[17]. **we chose to prioritize screening of the remaining six sites.** To validate these sites, we constructed a series of Y-to-F mutants. Strategically, as **the two amino acids Y111 and Y112 are adjacent and likely have identical physiological functions, we selected the double mutation at YY111/112.** While single mutations of several other tyrosine residues had minimal effects, double mutations of Y111 and Y112 specifically and significantly attenuated Src-mediated IRS4 phosphorylation (Fig. 2G). This was further confirmed under conditions of constitutive Src activation, where the YY111/112FF mutant had significantly attenuated phosphorylation levels despite the presence of Src (Y530F) (Fig. 2H). Finally, *in vitro* kinase assays using proteins purified from *E. coli* or 293T cells demonstrated that Src directly phosphorylates IRS4, with significantly reduced phosphorylation in the YY111/112FF mutant (Fig. 2I). In summary, it was determined that the two residues YY111/112 are the main phosphorylation sites targeted by Src. Sequence alignment across multiple vertebrate species revealed that the YY111/112 residues are highly conserved (Fig. S2B), suggesting a fundamental biological role in IRS4-mediated signaling. To facilitate our study, we generated a phosphosite-specific antibody pYY111/112 that recognized phosphorylated

IRS4 WT but not the YY111/112FF mutant, confirming its high specificity for pYY111/112 sites (Fig. 2J). Dot blot assays using synthetic peptides confirmed that both clones exhibit high affinity and strict specificity for the double-phosphorylated YY111/112 site (Fig. S2C). Collectively, these data indicate that Src mainly phosphorylates IRS4 at the conserved YY111/112 residues, and site-specific antibodies targeting YY111/112 phosphorylation provide a powerful tool for our subsequent studies.

Phosphorylation of IRS4 at YY111/112 is essential for its oncogenic functions in LUSC cells.

To investigate the role of tyrosine phosphorylation of IRS4 at YY111/112 in tumor progression, we first analyzed IRS4 expression in the TCGA database. The analysis revealed that *IRS4* mRNA levels were significantly upregulated in LUSC tissues compared with normal lung tissues (Fig. 3A), suggesting that IRS4 acts as an oncogenic driver in LUSC. To further investigate the role of the YY111/112 sites of the IRS4 protein in lung squamous cell carcinoma, we performed phenotypic analysis in H226, a LUSC cell line. Following the knockdown of endogenous IRS4 (Fig. S3A), stable cell lines were established by expressing IRS4-WT or IRS4-YY111/112FF (Fig. 3B). CCK-8 and colony formation assays revealed that IRS4 silencing markedly inhibited H226 cell proliferation and anchorage-dependent growth. Notably, these inhibitory effects were rescued by IRS4 WT but not the YY111/112FF mutant (Fig. 3C-D). These data indicate that YY111/112 phosphorylation is essential for the tumorigenic potential of LUSC cells.

In terms of motility, both wound-healing and Trans-well analyses showed that re-expression of IRS4-WT markedly promoted the migratory and invasive abilities of H226 cells, whereas IRS4-YY111/112FF mutant largely abolished these effects (Fig. 3E-F). Consistently, anchorage-independent growth assays demonstrated that phosphorylation at YY111/112 is essential for the clonogenic potential of individual cells, as the IRS4-YY111/112FF mutant failed to completely rescue colony formation (Fig. 3G). To further validate these observations, we used A549 cells lacking endogenous IRS4 expression to assess the gain-of-function effect of IRS4. Stable expression of IRS4-WT or IRS4-YY111/112FF mutants enables us to assess the IRS4 phenotype (Fig. S3B) more accurately. In line with the results obtained from H226 cells, IRS4-WT expression robustly enhanced A549 cell viability and colony formation; these growth-promoting effects were markedly attenuated in the IRS4-YY111/112FF stable cell line (Fig. S3C-D). Similarly, IRS4-WT induced a robust increase in A549 cell migration, an effect largely attenuated by the IRS4-YY111/112FF mutation (Fig. S3E-F). Soft-agar assays further confirmed that anchorage-independent growth in this IRS4-null background is critically dependent on YY111/112 phosphorylation, whereas the YY111/112FF mutant exhibited a markedly reduced capacity to support colony formation (Fig. S3G). Collectively, these data provide definitive evidences that IRS4 drives lung cancer cell proliferation, colony formation, and motility through a mechanism that is fundamentally dependent on tyrosine phosphorylation at the YY111/112 site.

Phosphorylation of IRS4 at YY111/112 promotes p85β recruitment and activates PI3K–AKT signaling

To elucidate the molecular mechanism by which IRS4 YY111/112 phosphorylation drives the malignant progression of LUSC, we performed immunoprecipitation and mass spectrometry (IP-MS) analysis on stable H226^{shIRS4}Flag-IRS4-WT and H226^{shIRS4}Flag-IRS4-YY111/112FF stable cell lines to identify differences in interacting proteins between IRS4-WT and IRS4-YY111/112FF mutant (Fig. 4A). Volcano plot analysis revealed that the expression and activity of key PI3K pathway components including p85β (PIK3R2) and PIK3CA in the IRS4-WT complex were significantly altered. At the same time, p85α (PIK3R1) did not show significant enrichment. Consistently, Gene Ontology (GO) and pathway enrichment analysis further confirmed that the differentially expressed proteins were predominantly associated with PI3K/AKT activation and GTP hydrolysis (Fig. 4B). Recruitment of the p85 regulatory subunit of PI3K is a key step in pathway activation[33]. Further analysis of paired clinical samples showed that the abundance of p85α was significantly reduced in tumor tissues compared with matched normal tissues, whereas the abundance of p85β was correspondingly increased (Fig. S4A). These suggest that p85β may be the major PI3K regulatory subunit involved by IRS4 in LUSC cancer.

Next, we investigated whether phosphorylation at the YY111/112 site is essential for IRS4-mediated downstream signaling. In H226^{shIRS4}Flag-IRS4-WT and H226^{shIRS4}Flag-IRS4-YY111/112FF stable cell lines, serum stimulation induced significant phosphorylation of IRS4 at the YY111/112 site in IRS4-WT expressing cells, accompanied by significant activation of the AKT and ERK signaling pathways. Conversely, AKT signaling activation was significantly attenuated in YY111/112FF mutant cells without affecting ERK signaling activation (Fig. 4C). These results demonstrate that YY111/112 phosphorylation is essential for the full-scale activation of the PI3K/AKT signaling node in LUSC cells. Co-immunoprecipitation assays further demonstrated that IRS4-WT efficiently associated with p85β in the presence of Src, whereas the YY111/112FF mutant exhibited reduced interaction with p85β (Fig. 4D). Furthermore, deletion of either the N-terminal or C-terminal SH2 domain of p85β markedly impaired its interaction with IRS4, while simultaneous deletion of both SH2 domains completely abolished binding confirming that SH2-mediated recognition is essential for p85β recruitment (Fig. S4B). Meanwhile, to evaluate the structural consequences of YY111/112 phosphorylation on the interaction between IRS4 and its downstream effector p85β, we used AlphaFold3 to generate structural models of the IRS4–WT/p85β complex and the corresponding phosphorylated IRS4–pYY111/112/p85β complex (Fig. 4E-F). Structural comparison revealed a pronounced conformational rearrangement in the phosphomimetic model. Upon alignment of the core scaffold of IRS4, the α-helical segment spanning residues C332–H360 underwent a substantial rigid-body reorientation relative to p85β, exhibiting an estimated rotational displacement of approximately 125°. This movement repositioned the helix toward the p85β interface, thereby expanding the contact surface. Concomitantly, residues P368–F399 adopted a more ordered α-helical conformation that projected toward p85β, further enlarging the interaction interface. Collectively, these structural changes appear to reposition the IRS4 C-terminal domain, broadening the interaction interface and creating a more favorable structural framework for p85β binding. Consistent with this

structural remodeling, Rosetta-based interface analysis demonstrated a marked increase in buried surface area, from 4043.74 Å² in the WT complex to 6613.52 Å² in the phosphomimetic complex[34]. In parallel, the predicted binding free energy was substantially reduced (ΔΔG = −934.24), indicative of enhanced complex stability.

To elucidate the interacting residues in greater depth, we analyzed the four YXXM motifs including Y779, Y700, Y717, or Y743 involved on IRS4 and the SH2 domain of p85β. Site-directed mutagenesis analysis showed that the Y779 mutation significantly weakened the IRS4 protein's ability to recruit p85β, indicating that the Y779 site is a key residue in these four YXXM motifs. Meanwhile, the combined mutation YY111/112FF and Y779F almost completely eliminated the interaction between IRS4 and p85β N-SH2 domain, thereby identifying these three residues as the key sites for IRS4 to recruit the p85β regulatory isoform (Fig. 4G). Additionally, Residue-level analysis revealed enhanced contacts between the p85β SH2 domain and IRS4, particularly involving residues Lys376 and Leu377 of p85β (Fig.S4C). Moreover, mutation of key residues within the p85β SH2 domain (KL376/377AA) significantly weakened IRS4 association (Fig. 4H). Collectively, these data demonstrate that phosphorylation of IRS4 at YY111/112 induces a conformational switch that enhances p85β binding via N-SH2-domain–dependent interactions, thereby promoting activation of the PI3K–AKT signaling pathway.

Various growth factors induce phosphorylation of IRS4 at YY111/112

To determine whether phosphorylation of IRS4 at YY111/112 responds to extracellular stimulation, H226^{shIRS4}-WT-IRS4 cells were subjected to serum starvation and stimulated with Insulin, IGF, EGF, or FBS. Immunoprecipitation and immunoblotting of phosphorylation-specific antibodies showed that YY111/112 phosphorylation could be induced by insulin, IGF, or EGF, with FBS showing more potent activation (Fig. 5A). Similar results were obtained in 293T cells, confirming that FBS potently induces IRS4 Y111/112 phosphorylation with different extracellular stimuli (Fig. 5B). Meanwhile, to further clarify whether YY111/112 phosphorylation depends on Src kinase activity, we treated H226^{shIRS4}-IRS4-WT cells and H226^{shIRS4}-IRS4-YY111/112FF cells with the Saracatinib. Saracatinib treatment significantly reduced FBS-induced YY111/112 phosphorylation, indicating that Src activity is essential for phosphorylation at YY111/112. Simultaneously, Src inhibition attenuated AKT activation, supporting a functional link between Src-mediated IRS4 phosphorylation and the downstream PI3K-AKT signaling pathway (Fig. 5C).

To further validate the role of the Src in regulation of IRS4, we used previously reported SYF cells lacking Src family kinases, Src, Fyn and Yes known to be redundantly expressed in tumors[35, 36]. Based on this, we constructed a SYF cell line stably overexpressing Src. SYF or SYF-Src cells were subjected to serum starvation and stimulated with insulin, IGF, EGF, or FBS. In line with H226 results, FBS stimulation significantly induced phosphorylation at the YY111/112 sites in SYF-Src cells (Fig. 5D). Compared to SYF-Src, the phosphorylation level of YY111/112 induced by 10% serum was attenuated in SYF cells. Obviously, we found that under different growth factor stimuli, the levels of both pAKT and pERK in SYF cells were significantly lower than those in SYF-Src cells. This also confirmed that Src, as a kinase, can

be activated by various receptor signals at the cell surface and participate in multiple cellular physiological activities[37]. Moreover, Saracatinib treatment significantly inhibited IRS4 YY111/112 phosphorylation in SYF-Src cells (Fig. 5E). These results collectively indicate that IRS4 YY111/112 phosphorylation is predominantly dependent on Src kinase.

Next, we performed pharmacological inhibition assays using the AKT pathway inhibitor MK2206 and the Src inhibitor saracatinib to further define the functional relevance of IRS4 phosphorylation at YY111/112. Treatment with MK2206 markedly suppressed clonogenic growth; however, a significant difference in colony-forming capacity persisted between IRS4-WT and IRS4-YY111/112FF expressing cells, indicating that the phosphorylation-deficient mutant remained partially impaired even under AKT inhibition. In contrast, saracatinib treatment significantly reduced clonogenesis in both WT and mutant groups, and notably, abolished the difference in colony formation between IRS4-WT and IRS4-YY111/112FF cells. These findings suggest that Src inhibition eliminates the functional advantage conferred by YY111/112 phosphorylation. Collectively, these data demonstrate that phosphorylation at YY111/112 promotes clonogenic growth in a Src–IRS4-pAKT dependent manner (Fig. 5F-G). Sequence alignment further showed that the YY111/112 site is conserved among IRS family members, highlighting its potential functional importance (Fig. 5H).

To explore whether YY111/112 phosphorylation affects IRS4 protein stability, we performed cycloheximide (CHX) chase assays. IRS4-WT and IRS4-YY111/112FF exhibited similar degradation patterns over the 48-hour time course, and quantitative analysis indicated no significant difference in protein half-life between the two constructs (Fig.5 SA-B). In addition, subcellular fractionation analysis demonstrated that the YY111/112FF mutation does not affect IRS4 subcellular localization, as both WT and mutant IRS4 were similarly distributed among cytoplasmic, membrane, and nuclear fractions (Fig. S5C-D). Together, these findings demonstrate that Src-mediated phosphorylation of IRS4 at YY111/112 enhances AKT activation and promotes colony-forming capacity without affecting IRS4 protein stability or subcellular localization.

pYY111/112 peptide blocks Src-IRS4 interaction and suppresses tumor growth.

To investigate the functional relevance of IRS4 YY111/112 phosphorylation *in vivo*, we constructed a Tat-coupled phosphopeptide containing the YY111/112 sequence[38, 39]. Fluorescence microscopy confirmed the efficient intracellular delivery of FITC-labeled peptides in H226 cells (Fig. 6A). Co-immunoprecipitation analysis revealed that peptide treatment dose-dependently disrupted the association between Src and IRS4 (Fig. 6B). To assess its biological significance *in vivo*, H226, $H226^{shIRS4}$, $H226^{shIRS4}$-IRS4-WT, or $H226^{shIRS4}$-IRS4-YY111/112FF stable cell lines were subcutaneously implanted into nude mice. Beginning on Day 14, mice received intratumoral injections of the Tat-conjugated phospho-peptide at the indicated intervals (Fig. 6C). Re-expression of IRS4-WT significantly enhanced tumor growth compared with shIRS4 cells. In contrast, the YY111/112FF mutant exhibited attenuated tumorigenicity (Fig. 6D-E). Notably, peptide treatment significantly suppressed tumor growth and reduced tumor weight in the IRS4-WT group but had minimal effect in the YY111/112FF group (Fig.

6E-F), supporting the specificity of this intervention for YY111/112-dependent signaling. Immunohistochemical analysis further revealed decreased pYY111/112 and Ki67 staining in peptide-treated IRS4-WT tumors (Fig. 6G), indicating reduced IRS4 phosphorylation and tumor cell proliferation *in vivo*. No significant differences in body weight were observed among groups (Fig. S6A), indicating an acceptable tolerability profile. Collectively, these findings demonstrate that YY111/112 phosphorylation is required for IRS4-driven tumor growth *in vivo*, and that pYY111/112-containing cell-permeable phosphopeptide effectively impairs Src-IRS4–p85β signaling and tumor progression without toxicity.

YY111/112 phosphorylation is positively correlated with human LUSC progression.

To evaluate the clinical relevance of IRS4 and its phosphorylation at YY111/112 in LUSC, we examined their expression patterns using a LUSC tumor tissue microarray. Representative immunohistochemical staining demonstrated that both total IRS4 and phosphorylated IRS4 at Y111/112 were markedly increased in tumor tissues compared with normal lung samples (Fig. 7A). Quantitative analysis using the H-score confirmed that the levels of IRS4 and pYY111/112 were significantly elevated in LUSC tissue compared to matched normal tissue (Fig. 7B-C). Notably, the high level of pYY111/112 was particularly pronounced in malignant tissue, suggesting that it may be a characteristic feature of lung squamous cell carcinoma pathology. We further evaluated whether the IRS4 signaling pathway is associated with disease severity. Comparison of H scores across clinical stages revealed significantly elevated levels of total IRS4 and pYY111/112 in advanced squamous cell carcinoma (stage III-IV) samples compared with early-stage (stage I-II) samples (Fig. 7D-E). These data indicate that hyperphosphorylation of IRS4 on the YY111/112 site is positively correlated with tumor progression and clinical malignancy.

Consistent with our previous results shown as Fig. 2 that Src and RPTPα are major regulators at the YY111/112 site, we analyzed their protein abundance in lung squamous cell carcinoma samples using the CPTAC database. This large-scale proteomics analysis revealed a significant reciprocal relationship: Src kinase was upregulated in LUSC tumors (Fig. 7F), whereas the phosphatase RPTPα was downregulated (Fig. 7G). This imbalance between the kinase and its phosphatase underlies the persistent hyperphosphorylation of IRS4 observed in patient samples. In summary, these clinical findings support a working model in which increased Src activity and loss of RPTPα drive hyperphosphorylation of IRS4 at YY111/112. This phosphorylation event facilitates the recruitment of the p85β subunit of PI3K, triggering robust AKT signaling and subsequently promoting the uncontrolled cell proliferation and tumorigenesis observed in LUSC (Fig. 7H).

DISCUSSION

In this study, we delineate a regulatory mechanism by which IRS4 promotes the progression of lung squamous cell carcinoma. We demonstrate that the tyrosine kinase Src directly phosphorylates IRS4 at the conserved YY111/112 sites. Phosphorylation at YY111/112 residues induces conformational

changes that enhance the ability of IRS4 to recruit the PI3K regulatory subunit p85β. Conversely, the phosphatase RPTPα counteracts this modification by dephosphorylating pYY111/112, thereby may reverse IRS4-mediated PI3K/AKT engagement. Importantly, analysis of LUSC tissue microarrays revealed that phosphorylation of IRS4 at Y111/112 is positively correlated with malignant tumor progression (Fig. 7). Within the IRS protein family, IRS1 and IRS2 are broadly expressed across most human tissues, whereas IRS4 exhibits a more restricted, tissue-specific expression pattern[12]. Although the YY111/112 site is conserved among IRS family members, its functional relevance has remained largely unexplored. Our data show that phosphorylation of this site can be induced by multiple growth factors, suggesting that it may represent a general regulatory node for signal integration. This observation raises the possibility that similar phosphorylation-dependent mechanisms may exist in other IRS proteins under specific cellular contexts. Additionally, the PhosphoSite database indicates that tyrosine phosphorylation of IRS4 has been reported predominantly in the C-terminal domain, whereas phosphorylation events in the PH and PTB domains have been infrequently reported and remain poorly characterized[15, 32]. Our findings suggest that phosphorylation at YY111/112 represents an underexplored regulatory modification in IRS signaling.

Given the central role of IRS4 as a docking adaptor for PI3K signaling, we also examined whether specific PI3K regulatory subunits are differentially involved downstream of YY111/112 phosphorylation. In our proteomic analysis, only p85β exhibited a significant change, whereas p85α remained largely unaffected. This finding supports that PI3K signaling in LUSC may preferentially depend on p85β rather than p85α[40]. Although p85α is broadly expressed and contributes to basal PI3K regulation, its abundance appears relatively stable and less responsive to IRS4-dependent signaling alterations[41]. In contrast, p85β has been reported to exhibit greater signaling flexibility and a stronger tendency to associate with phosphorylated adaptor proteins, features that are closely linked to sustained PI3K activation in tumor cells[33]. Consistent with this notion, phosphorylation of IRS4 at YY111/112 may selectively promote recruitment of p85β, thereby favoring formation of signaling-competent PI3K complexes without requiring measurable changes in p85α levels. These intrinsic differences between p85β and p85α provide a plausible explanation for the selective detection of p85β alterations in our proteomic data and support the view that p85β plays a more active role in driving PI3K pathway signaling and malignant proliferation[42, 43] .

Beyond identifying Src-mediated IRS4 phosphorylation, our findings also implicate the phosphatase RPTPα as an additional layer of regulation, whose role in cancer remains controversial. Several studies have reported that RPTPα promotes tumor progression by dephosphorylating Src at the inhibitory Y527 residue, thereby enhancing Src kinase activity[28, 29]. In contrast, other reports have suggested a tumor-suppressive function for RPTPα, particularly in breast cancer models, where RPTPα expression has been associated with reduced malignant behavior[44, 45]. In our results, we demonstrate that RPTPα dephosphorylates IRS4, providing new insights into the complexity of RPTPα-mediated signaling. These findings raise the possibility that RPTPα may exert context-dependent or dual functions in tumor cells. Specifically, RPTPα may simultaneously promote oncogenic signaling by activating Src through dephosphorylation at Y527, while attenuating downstream signaling by dephosphorylating IRS4 and

limiting PI3K pathway engagement. Such dual regulation may underlie the context-dependent effects of RPTPα in cancer.

Although our study provides mechanistic insight into the role of IRS4 YY111/112 phosphorylation in lung squamous cell carcinoma, several important questions remain to be addressed. It will be necessary to determine whether kinases other than Src can also regulate phosphorylation at the YY111/112 site. Furthermore, the functional role of IRS4 YY111/112 phosphorylation in normal tissues with high IRS4 expression, including embryonic and thymic cells, remains unclear, and its potential involvement in embryonic and T-cell developmental programs warrants further investigation.

In conclusion, we identify YY111/112 as a novel Src-mediated phosphorylation site on IRS4 that enhances p85β recruitment and correlates with tumor malignancy, providing new insight into adaptor protein regulation and a potential therapeutic avenue in lung squamous cell carcinoma.

MATERIALS AND METHODS

Cell line and cell Cell transfection

Human H226, A549, HEK-293T, and HEK-293FT cell lines were obtained from American Type Culture Collection (ATCC). SYF cell line was obtained from the China Center for Type Culture Collection (Wuhan, China). All cell lines were authenticated by short tandem repeat (STR) profiling before use. A549, HEK-293T, and HEK-293FT cells were maintained in DMEM, and H226 were maintained in RPMI-1640 medium (Corning), supplemented with 10% fetal bovine serum (Yeasen) and 1% penicillin/streptomycin (Yeasen) at 37°C in a humidified atmosphere containing 5% CO_2. For growth factor stimulation experiments, cells were serum-starved in DMEM or RPMI-1640 without serum for 24 h before stimulation. Transient transfection was performed using Vazyme Transfection Reagent (#7E603K2).

Antibodies and reagents

Antibodies against Src (#2109), Myc (#2276), pS473-AKT (#4060), AKT1 (#2967), ERK1/2 (#9102S), and pERK1/2 (#4370S) were from Cell Signaling Technology. Antibodies against RPTPα (#13079), GAPDH (#HRP-60004) and Alpha-Tubulin (#66031-1-Ig), GST (66001-2-Ig), N-cadherin(66219-1-Ig) and Lamin B1 (66095-1-Ig) were from ProteinTech. Antibodies against IRS4 (#R06849) and Flag (F1804) were from Sigma-Aldrich. Anti-normal mouse IgG antibody (#sc-2025) and Anti-normal rabbit IgG (#sc-2027) were from Santa Cruz Biotechnology. Anti-pTyr 4G10 antibody (#3168706) was from Millipore, Anti-HA antibody (MMS-101R) was from Covance. Epidermal growth factor (Roche), Insulin (Sigma), Insulin-like Growth Factor-1 (Sigma). Puromycin (#P8833), cycloheximide (CHX), and EDTA-free Protease Inhibitor Cocktail were from Sigma-Aldrich. Saracatinib (#AZD0530) was purchased from Selleck. MK2206 (#SF2712) was purchased from Biotime.

Antibodies against the IRS4 site-specific antibody (1:1000 for WB and 1:200 for IHC) were generated from Signalway Antibody LLC (Nanjing, China). Briefly, the IRS4 phosphopeptide

CAPDARLE(p)Y(p)YENARK conjugated with KLH and non-phosphopeptide CAPDARLEYYENARK were synthesized, respectively. The serum antibody was produced by immunizing rabbits with the synthetic phosphopeptide CAPDARLE(p)Y(p)YENARK after five immunizations. Non-phospho-specific antibodies were removed by chromatography using non-phosphopeptide CAPDARLEYYENARK. IRS4-pYY111/112 site-specific antibody was purified by affinity chromatography using epitope-specific CAPDARLE(p)Y(p)YENARK phosphopeptide.

Plasmids

FPC1-Myc-IRS4 was gifted from Prof. Gaofeng Fan, ShanghaiTech University, Shanghai, China. Using FPC1-Myc-IRS4 as a template, we further constructed IRS4-YY111/112FF, IRS4-Y700F, IRS4-Y717F, IRS4-Y743F, and IRS4-Y808F mutants by using the KOD-plus-mutagenesis Kit (TOYOBO) according to the manufacturer's protocol. The IRS4 truncated mutants lacking PH domain（1–200AA）, PTB domain（200–400AA）or C-domain（400–1257AA） were cloned into the vector pET-28a (Novagen) for the bacterially-expressed His-Tag protein. The Flag-Src, HA-Src, and GST-Src plasmids were described previously[46, 47]. The Human PI3KR2(p85β) gene was amplified by KOD-plus Kit (TOYOBO) using human cDNA made from HEK293T cell and then subsequently cloned into pCMV-Myc. Mutated p85β was introduced by using the KOD-plus-mutagenesis Kit (TOYOBO) according to the manufacturer's protocol. All the primers and oligos used for molecular cloning were listed in Table S1.

shRNA knockdown

The two IRS4 shRNA oligonucleotide sequences were obtained from the Thermo Fisher Scientific website and subcloned into the pLKO.1 vector. HEK293FT cells were used for virus packaging. pMD2G, pCMV-dR8, and shRNA plasmids were co-transfected into HEK293FT cells with Vazyme transfection reagents. The cell culture suspension containing the virus was collected 48 h after transfection. The H226 cells were infected and selected with puromycin (Yeasen) for 3 d.

IRS4 shRNA-1(3'-UTR):
5′-CCGGGCGCTACAGTCTACAGTGTTACTCGAGTAACACTGTAGACTGTAG CGCTTTTTG-3′
IRS4 shRNA-2 (3'-UTR):

5′-CCGGGGTCATTGTCTAATGATTCGACTCGAGTCGAATCATTAGACAATGA CCTTTTTG-3′

Protein expression and purification

Plasmids encoding His-tagged IRS4 truncations pET-28a-IRS4-PH, pET-28a-IRS4-PTB, or pET-28a-IRS4-C-terminal domains were transformed into *E.coli* BL21 competent cells. Protein expression was induced with 0.5 mM isopropyl β-d-1-thiogalactopyranoside (IPTG) for 12–16 h at 16 °C. Following induction, bacteria were harvested and lysed via sonication in lysis buffer (50 mM Tris-HCl, pH 8.0, 300 mM NaCl).

The His-tagged proteins were purified using Ni^{2+}-NTA Agarose (QIAGEN) according to the manufacturer's instructions. Briefly, the lysates were incubated with Ni^{2+}-NTA agarose beads under gentle agitation, followed by three washes with washing buffer (50 mM Tris-HCl, pH 8.0, 10 mM imidazole). The bound proteins were subsequently eluted with elution buffer (50 mM Tris-HCl, pH 8.0, 200 mM imidazole) and analyzed by western blotting[29].

Plasmid encoding GST-tagged Src or its truncated mutants pGEX-4T1-Src, pEGX-4T1-Src(ΔSH4), pEGX-4T1-Src(ΔSH3), pEGX-4T1-Src(ΔSH2), pEGX-4T1-Src(ΔSH1) was transformed into *E.coli* BL21 competent cells. Protein expression was induced with 0.5 mM isopropyl β-d-1-thiogalactopyranoside (IPTG) for 12–16 h at 16 °C. The resulting cell pellets were resuspended in lysis buffer (50 mM Tris-HCl, pH 7.4, 150 mM NaCl) and disrupted via sonication. The lysate was clarified by centrifugation at a speed of 16000×g for 20 min at 4°C, and the supernatant was loaded onto a column containing GST-Sefinose Resin (Sangon) to capture the GST-fusion proteins. After washing three times with wash buffer, the bound proteins were eluted using glutathione (GSH) buffer (50 mM Tris-HCl, pH 8.0, 20 mM GSH). The purity and identity of the proteins were verified by Coomassie Brilliant Blue staining and western blotting

***in vitro* kinase (IVK) assay**

Three IRS4 truncation proteins carrying HA and His tags, together with GST-Src, were purified and subjected to *in vitro* kinase assay in buffer containing 50 mM Tris-HCl, pH 7.4, 150 mM NaCl, 10 mM $MgCl_2$, and 2 mM DTT. Reactions were initiated by the addition of 1 mM ATP and incubated at room temperature for 1 h. The reactions were terminated by adding 5× SDS loading buffer, and samples were analyzed by immunoblotting using anti-phosphotyrosine, anti-HA, or anti-GST antibody.

Immunoprecipitation (IP) and Co-Immunoprecipitation (Co-IP)

HEK293T or H226 cells were transfected with the indicated expression plasmids for 48 h. Cells were harvested and lysed in either RIPA lysis buffer (50 mM Tris-HCl, pH 7.4, 150 mM NaCl, 0.05 % SDS, 1 % NP-40, 1 mM Na_3VO_4, 1 mM NaF, and protease inhibitor cocktail) for IP assays or Co-IP lysis buffer (50 mM Tris-HCl, pH 7.4, 150 mM NaCl, 10% glycerol, 1% NP-40, and protease inhibitor cocktail) for Co-IP assays, followed by sonication. After centrifugation at 16,000 × g for 30 min at 4°C, the supernatants were collected as whole-cell lysates. For each assay, 1 mg of total protein was incubated with 20 μL of protein A/G beads (Santa Cruz) and 1 μg of the indicated primary antibody overnight at 4°C. The beads were washed five times with the corresponding lysis buffer, mixed with 2× protein loading buffer, and boiled for 10 min. The resulting samples were analyzed by western blotting.

Western blotting (WB)

Cell lysates or protein samples were mixed with 5× protein loading buffer (Sangon), boiled for 10 min, and briefly centrifuged before loading onto SDS-PAGE gels. After electrophoresis, proteins were

transferred onto 0.45 μm PVDF membranes. Membranes were blocked in 5% BSA prepared in TBS containing 0.1% Tween-20 (TBST) for 1 h at room temperature and then incubated with primary antibodies overnight at 4°C. After three washes with TBST, membranes were incubated with HRP-conjugated secondary antibodies for 1 h at room temperature. Membranes were washed three additional times with TBST and developed using ECL detection reagents (Tanon). Signals were visualized using an Amersham Imager (GE Healthcare).

Cell counting kit 8 (CCK-8) assay

H226 or A549 cells were transduced with the indicated lentiviruses and subjected to selection for 7 d to generate knockdown or overexpression variants. For the cell proliferation assay, cells were seeded into 96-well plates at a density of 1×10^3 cells per well in 100 μL of medium. At the designated time points, 10 μL of Cell Counting Kit-8 solution (CCK-8, Yeasen, China) was added to each well. Following 1 h incubation, the optical density (OD) at 450 nm was measured using a microplate reader to evaluate cell viability in accordance with the manufacturer's protocol.

Colony formation assay

For colony formation assays, H226 or A549 stable cells were seeded per well in triplicate into six-well plates and cultured in DMEM or RPMI-1640 medium containing 10% FBS for 2–3 weeks. Colonies were fixed with 10% formaldehyde, stained with 1% crystal violet, and quantified using ImageJ.

Soft agar colony formation assay

For soft agar assays, equal volumes of 1.2% low-melting-point agarose and 2× DMEM or 2× RPMI-1640 supplemented with 10% FBS and antibiotics were mixed and used as the bottom layer in six-well plates. After solidification, 1×10^3 cells were suspended in 0.7% agar containing 10% FBS and antibiotics and overlaid onto the base layer. Plates were incubated at 37°C in a humidified incubator with 5% CO_2 for 2–3 weeks. Colonies were then stained with 0.005% crystal violet, imaged, and quantified using ImageJ.

Wound healing assays

Wound healing assays were performed using culture inserts (IBIDI) according to the manufacturer's instructions. Cells were seeded at a density of 3×10^4 cells per well and allowed to adhere overnight. The inserts were then removed, and the medium was replaced with DMEM containing 1% FBS. Wound closure was monitored microscopically, and representative images were acquired at the indicated time points.

Subcellular fractionation

H226 cells stably expressing Flag-tagged WT IRS4 or YY111/112FF mutant were harvested and resuspended in buffers supplemented with protease inhibitors. Subcellular fractionation was performed using the Membrane and Cytosol Protein Extraction Kit and the Nuclear and Cytoplasmic Protein Extraction Kit (Yeasen, Shanghai, China) according to the manufacturer's protocols to isolate cytoplasmic, membrane, and nuclear fractions[48]. To evaluate the subcellular localization of IRS4 and ensure the purity of the isolated fractions, Western blot analysis was conducted using compartment-specific markers.

Peptide Preparation

The cell-permeable phosphopeptide pYY111/112-TAT was designed based on the IRS4 sequence, incorporating dual phosphorylation at Tyr111 and Tyr112 (ADAPARLEpYpYENAR). The peptide was N-terminally labeled with FITC and conjugated to the HIV-TAT protein transduction domain (YGRKKRRQRRR) to ensure efficient intracellular delivery (sequence: FITC-ADAPARLEpYpYENAR-YGRKKRRQRRR; MW: 3843.05 Da).

The peptide was custom-synthesized by Signalway Antibody LLC (Nanjing, China) with a chromatographic purity exceeding 95%. Lyophilized peptides were stored at -20 °C to prevent degradation. For *in vitro* assays, the peptide was reconstituted in sterile phosphate-buffered saline (PBS) to generate a 25 mM stock solution. For *in vivo* administration, the peptide was dissolved in PBS at a concentration of 1 mg/mL and maintained on ice prior to injection.

Xenograft tumour model

All animal experimental procedures were performed in accordance with the guidelines and with the approval of the Shanghai Jiao Tong University Medical Animal Ethics Committee. Male BALB/c nude mice (7-weeks-old) were maintained under specific pathogen-free (SPF) conditions in a 12-h light/dark cycle at 20-22°C and 40 % relative humidity, with ad libitum access to a standard chow diet (Xietong Shengwu, Cat# XTC01WC-001). To establish the subcutaneous xenograft model, 4×10^6 H226 cells were suspended in PBS and injected into the right flank of each mouse. Once the tumors reached a visible size (14 d post-inoculation), mice were randomly assigned to the indicated treatment groups. The treatment group received intratumoral (i.t.) injections of the pYY111/112-TAT peptide (10 ug per dose) every other day for 16 consecutive days. Tumor scales were monitored longitudinally using digital calipers, and volumes were calculated using the formula: V = 0.5×length × width^2. At the study endpoint, mice were euthanized, and tumors were harvested, weighed, and processed for subsequent biochemical analysis.

Immunofluorescence

For immunofluorescence analysis, H266 cells were seeded onto glass coverslips in 24-well plates at 40% confluency and incubated with 10 uM peptide for 1 h. Following three washes with PBS, the cells were fixed with ice-cold methanol at 4 °C. After further washing, the coverslips were blocked and

permeabilized with TBS containing 1% BSA and 0.1% Triton X-100 for 15 min. Nuclei were subsequently counterstained with Hoechst (Thermo Fisher) for 15 min in the dark. Finally, the coverslips were washed, mounted using ProLong™ Antifade Mountant, and sealed with nail polish. Fluorescence images were captured using Pano Cube (MeCA Scientific).

Immunohistochemical staining (IHC)

A lung squamous cell carcinoma (LUSC) tissue microarray containing 60 paired LUSC tissues and corresponding adjacent normal lung tissues (Cat#HLugS120CS01, Superchip, China) was used for immunohistochemical analysis. IHC staining was performed according to the manufacturer's instructions using antibodies against IRS4 (1:200, Sigma) or pYY111/112 (1:200, SAB). A staining index score was calculated by multiplying the staining intensity score by the extent score. Staining intensity was graded as 0 (no staining), 1 (weak), 2 (moderate), or 3 (strong). The extent of staining was scored according to the percentage of positive cells as follows: 0, 0–5%; 1, 5–25%; 2, 26–50%; 3, 51–75%; and 4, 76–100%. The final staining index ranged from 0 to 12.

The histochemistry score (H-score) was calculated based on both the percentage and staining intensity of positive cells using the following formula: H-score = Σ(pi × i), where *i* represents the staining intensity (0–3) and *pi* represents the percentage of cells at each intensity level. Accordingly, the H-score was defined as: (percentage of weakly stained cells × 1) + (percentage of moderately stained cells × 2) + (percentage of strongly stained cells × 3).

Structural modeling and analysis

Structural modeling of the IRS4–p85β complex was performed using AlphaFold3 (AF3). Two types of complexes were generated including the WT-IRS4/p85β and pYY111/112-IRS4/p85β forms. To ensure consistency in conformational sampling and reproducibility, all predictions were carried out on the AlphaFold3 server using a fixed random seed (12345), and the predicted structures were exported in CIF format[49]. The resulting models were visualized and initially inspected in PyMOL. Protein–protein interaction interfaces were further analyzed using custom scripts implemented in PyRosetta, which were used to calculate interface binding free energy (ΔG), buried surface area (BSA), and interfacial residue composition[34]. In addition, the Gemmi library was used to measure distances between key interfacial atoms for structural analysis[50].

Identification of phosphosite by Mass Spectrometry

Full-length IRS4 was divided into three truncated mutants for phosphorylation site mapping. Each truncated mutant was subjected to an *in vitro* kinase assay with recombinant Src protein. Following the reaction, one-tenth of each sample was collected for western blot analysis to evaluate overall phosphorylation, and the remaining reaction products were subjected to phosphor-peptide analysis. Samples were digested and analyzed on Orbitrap Fusion Lumos mass spectrometer (Thermo Fisher

Scientific, Waltham, MA, USA). Raw mass spectrometry data were processed using PEAKS Studio to identify phosphorylation sites.

Identification of interacting proteins by Mass spectrometry

H226 cells stably expressing Flag-tagged WT-IRS4 or the YY111/112FF mutant were cultured in 10-cm dishes until confluent. Cells were harvested and lysed in Co-IP lysis buffer containing 50 mM Tris-HCl, pH7.4, 150 mM NaCl, 10% glycerol, 1% NP-40, and protease inhibitor cocktail. Lysates were incubated with anti-Flag affinity beads (CST) at 4°C overnight to enrich Flag-IRS4-associated protein complexes. After incubation, the beads were washed five times with Co-IP lysis buffer, and bound proteins were eluted by boiling in 100 µL of 2% SDS for 10 min. Two independent biological replicates from each group were subjected to mass spectrometry analysis to identify IRS4-associated proteins.

MS experiments were performed using an Orbitrap Fusion Lumos mass spectrometer (Thermo Fisher Scientific, Waltham, MA, USA) coupled to an EASY-nLC 1200 system via an EASY-Spray ion source (Thermo Fisher Scientific). Precursor ions selected for MS/MS were isolated in the quadrupole with an isolation window of 4 Da and fragmented by higher-energy collisional dissociation (HCD) at a normalized collision energy of 30% ± 5%. MS/MS spectra were analyzed using PEAKS 10.0 (Bioinformatics Solutions) for data processing, *de novo* sequencing, and database searching against the UniProt human proteome database. False discovery rate (FDR) estimation was enabled. Peptides were filtered at −log10(P value) ≥ 20, and proteins were filtered at −log10 (P value) ≥ 15 with at least one unique peptide. These settings yielded an FDR < 1% at the peptide-spectrum match level in all experiments. Proteins sharing significant peptide evidence were grouped into clusters. MS-based proteomic analysis was performed at the Proteomics Core Facility, School of Basic Medical Sciences, Shanghai Jiao Tong University School of Medicine. The resulting mass spectrometry data were further analyzed using Perseus v2.1.3.0 and visualized in GraphPad Prism 9.

Statistical Analysis

Statistical analyses were performed using GraphPad Prism 9 software. Data are presented as mean ± SD unless otherwise specified. Error bars indicate SD from at least three independent experiments. Differences between two groups were assessed using a two-tailed Student's *t*-test for unpaired data or a Wilcoxon matched-pairs signed-rank test for paired data, as appropriate. Comparisons among multiple groups were analyzed using one-way or two-way ANOVA, as indicated in the figure legends. Statistical significance was defined as *P <0.05, **P <0.01, ***P <0.001, and ****P <0.0001.

Declarations

DATA AVAILABILITY

The mass spectrometry data generated in this study have been uploaded to Integrated Proteome Resources (iProX) database under the accession number IPX001474300 and IPX0014773000. Source

data are provided with this paper. The remaining data are available within the Article, Supplementary Information or Source Data file.

ACKNONWLEDGEMENTS
We sincerely thank Professor Gaofeng Fan for his generous support with plasmids and antibodies. We are grateful to Dr. Yanchun Zhang, Dr. Caihu Huang, Dr. Zihan Zhou, and Dr. Hongyan Li for their technical assistance. We also thank the Mass Spectrometry Platform of Shanghai Jiao Tong University School of Medicine for technical support. This work was supported by the National Natural Science Foundation of China (No. 82073043 to J.H.).

AUTHOR CONTRIBUTIONS
J.H. and J.Y. supervised the project. J.H. and Y.A. conceived and designed the experiments. Y.A. performed most of the experiments. Q.R. performed the AlphaFold analysis. Y.A. and Q.R. contributed equally to this work. X.J., W.K., R.C., Y.W., G.Y. and X.Z. provided technical assistance and contributed to the experiments. J.H., J.Y., G.Y. and Y.A. analyzed and discussed the data. J.H. and Y.A. wrote the manuscript.

COMPETING INTERESTS

The authors declare no competing interests.

References

1. Wang M, Herbst RS, Boshoff C. Toward personalized treatment approaches for non-small-cell lung cancer. *Nat Med* 2021; 27: 1345–1356.
2. Cancer Genome Atlas Research N. Comprehensive genomic characterization of squamous cell lung cancers. *Nature* 2012; 489: 519–525.
3. Gandara DR, Hammerman PS, Sos ML, Lara PN, Hirsch FR. Squamous cell lung cancer: from tumor genomics to cancer therapeutics. *Clinical Cancer Research : an Official Journal of the American Association For Cancer Research* 2015; 21: 2236–2243.
4. Rodon J, Dienstmann R, Serra V, Tabernero J. Development of PI3K inhibitors: lessons learned from early clinical trials. *Nat Rev Clin Oncol* 2013; 10: 143–153.
5. Hoxhaj G, Manning BD. The PI3K-AKT network at the interface of oncogenic signalling and cancer metabolism. *Nat Rev Cancer* 2019; 20: 74–88.
6. Du Z, Lovly CM. Mechanisms of receptor tyrosine kinase activation in cancer. *Mol Cancer* 2018; 17: 58.
7. Shyam Sunder S, Sharma UC, Pokharel S. Adverse effects of tyrosine kinase inhibitors in cancer therapy: pathophysiology, mechanisms and clinical management. *Signal Transduction and Targeted*

Therapy 2023; 8: 262.

8. Weischenfeldt J, Dubash T, Drainas AP, Mardin BR, Chen Y, Stütz AM *et al*. Pan-cancer analysis of somatic copy-number alterations implicates IRS4 and IGF2 in enhancer hijacking. *Nat Genet* 2016; 49: 65–74.
9. Zhang Y, Chen F, Fonseca NA, He Y, Fujita M, Nakagawa H *et al*. High-coverage whole-genome analysis of 1220 cancers reveals hundreds of genes deregulated by rearrangement-mediated cis-regulatory alterations. *Nat Commun* 2020; 11: 736.
10. Taniguchi CM, Emanuelli B, Kahn CR. Critical nodes in signalling pathways: insights into insulin action. *Nature Reviews Molecular Cell Biology* 2006; 7: 85–96.
11. Lavan BE, Fantin VR, Chang ET, Lane WS, Keller SR, Lienhard GE. A novel 160-kDa phosphotyrosine protein in insulin-treated embryonic kidney cells is a new member of the insulin receptor substrate family. *J Biol Chem* 1997; 272: 21403–21407.
12. Mardilovich K, Pankratz SL, Shaw LM. Expression and function of the insulin receptor substrate proteins in cancer. *Cell Communication and Signaling : CCS* 2009; 7: 14.
13. Myers MG, Mendez R, Shi P, Pierce JH, Rhoads R, White MF. The COOH-terminal tyrosine phosphorylation sites on IRS-1 bind SHP-2 and negatively regulate insulin signaling. *J Biol Chem* 1998; 273: 26908–26914.
14. Ikink GJ, Boer M, Bakker ERM, Hilkens J. IRS4 induces mammary tumorigenesis and confers resistance to HER2-targeted therapy through constitutive PI3K/AKT-pathway hyperactivation. *Nat Commun* 2016; 7: 13567.
15. Guijarro LG, Justo Bermejo FJ, Boaru DL, De Castro-Martinez P, De Leon-Oliva D, Fraile-Martínez O *et al*. Is Insulin Receptor Substrate4 (IRS4) a Platform Involved in the Activation of Several Oncogenes? *Cancers* 2023; 15.
16. Qiu H, Zappacosta F, Su W, Annan RS, Miller WT. Interaction between Brk kinase and insulin receptor substrate-4. *Oncogene* 2005; 24: 5656–5664.
17. Zhang Y, Xiong X, Zhu Q, Zhang J, Chen S, Wang Y *et al*. FER-mediated phosphorylation and PIK3R2 recruitment on IRS4 promotes AKT activation and tumorigenesis in ovarian cancer cells. *Elife* 2022; 11.
18. Fantin VR, Keller SR, Lienhard GE, Wang LM. Insulin receptor substrate 4 supports insulin- and interleukin 4-stimulated proliferation of hematopoietic cells. *Biochem Biophys Res Commun* 1999; 260: 718–723.
19. Escribano O, Fernández-Moreno MD, Zueco JA, Menor C, Fueyo J, Ropero RM *et al*. Insulin receptor substrate-4 signaling in quiescent rat hepatocytes and in regenerating rat liver. *Hepatology (Baltimore, Md)* 2003; 37: 1461–1469.
20. Cuevas EP, Escribano O, Chiloeches A, Ramirez Rubio S, Román ID, Fernández-Moreno MD *et al*. Role of insulin receptor substrate-4 in IGF-I-stimulated HEPG2 proliferation. *J Hepatol* 2007; 46: 1089–1098.

21. Wang X, Liu Y, Zhao Q, Wang X, Chen X, Hou L *et al*. PILRB potentiates the PI3K/AKT signaling pathway and reprograms cholesterol metabolism to drive gastric tumorigenesis and metastasis. *Cell Death Dis* 2024; 15: 642.
22. He Y, Sun MM, Zhang GG, Yang J, Chen KS, Xu WW *et al*. Targeting PI3K/Akt signal transduction for cancer therapy. *Signal Transduction and Targeted Therapy* 2021; 6: 425.
23. Yeatman TJ. A renaissance for SRC. *Nat Rev Cancer* 2004; 4: 470–480.
24. Pelaz SG, Tabernero A. Src: coordinating metabolism in cancer. *Oncogene* 2022; 41: 4917–4928.
25. Zhang S, Yu D. Targeting Src family kinases in anti-cancer therapies: turning promise into triumph. *Trends Pharmacol Sci* 2011; 33: 122–128.
26. Delaveris CS, Loudermilk RP, Pandey A, Remesh SG, Peters-Clarke TM, Ganjave SD *et al*. Autophagolysosomal exocytosis inverts Src kinase onto the cell surface in cancer. *Science (New York, NY)* 2026; 391: eaec1778.
27. Zheng XM, Wang Y, Pallen CJ. Cell transformation and activation of pp60c-src by overexpression of a protein tyrosine phosphatase. *Nature* 1992; 359: 336–339.
28. Su J, Muranjan M, Sap J. Receptor protein tyrosine phosphatase alpha activates Src-family kinases and controls integrin-mediated responses in fibroblasts. *Current Biology : CB* 1999; 9: 505–511.
29. Fang J, Zhang Y, Huang C, Lu R, Yu J, Chen R *et al*. Glucose-mediated N-glycosylation of RPTPα affects its subcellular localization and Src activation. *Oncogene* 2023; 42: 1058–1071.
30. Flint AJ, Tiganis T, Barford D, Tonks NK. Development of "substrate-trapping" mutants to identify physiological substrates of protein tyrosine phosphatases. *Proc Natl Acad Sci U S A* 1997; 94: 1680–1685.
31. Buist A, Blanchetot C, Tertoolen LG, den Hertog J. Identification of p130cas as an in vivo substrate of receptor protein-tyrosine phosphatase alpha. *J Biol Chem* 2000; 275: 20754–20761.
32. Hornbeck PV, Zhang B, Murray B, Kornhauser JM, Latham V, Skrzypek E. PhosphoSitePlus, 2014: mutations, PTMs and recalibrations. *Nucleic Acids Res* 2014; 43: D512–D520.
33. Vallejo-Díaz J, Chagoyen M, Olazabal-Morán M, González-García A, Carrera AC. The Opposing Roles of PIK3R1/p85α and PIK3R2/p85β in Cancer. *Trends in Cancer* 2019; 5: 233–244.
34. Alford RF, Leaver-Fay A, Jeliazkov JR, O'Meara MJ, DiMaio FP, Park H *et al*. The Rosetta All-Atom Energy Function for Macromolecular Modeling and Design. *J Chem Theory Comput* 2017; 13: 3031–3048.
35. Klinghoffer RA, Sachsenmaier C, Cooper JA, Soriano P. Src family kinases are required for integrin but not PDGFR signal transduction. *EMBO J* 1999; 18: 2459–2471.
36. Ali R, Saleh MY, Amshawee AM, Alshamsi HA, Al-Nayili A, Oleiwi BM *et al*. Recent advances in rice-derived heterogeneous catalysts for green organic synthesis. *Mol Divers* 2026.
37. Thomas SM, Brugge JS. Cellular functions regulated by Src family kinases. *Annu Rev Cell Dev Biol* 1997; 13: 513–609.

38. Wang L, Wang N, Zhang W, Cheng X, Yan Z, Shao G *et al*. Therapeutic peptides: current applications and future directions. *Signal Transduction and Targeted Therapy* 2022; 7: 48.
39. Wang Y, Shu H, Qu Y, Jin X, Liu J, Peng W *et al*. PKM2 functions as a histidine kinase to phosphorylate PGAM1 and increase glycolysis shunts in cancer. *EMBO J* 2024; 43: 2368–2396.
40. Vallejo-Díaz J, Olazabal-Morán M, Cariaga-Martínez AE, Pajares MJ, Flores JM, Pio R *et al*. Targeted depletion of PIK3R2 induces regression of lung squamous cell carcinoma. *Oncotarget* 2016; 7: 85063–85078.
41. Luo J, Field SJ, Lee JY, Engelman JA, Cantley LC. The p85 regulatory subunit of phosphoinositide 3-kinase down-regulates IRS-1 signaling via the formation of a sequestration complex. *J Cell Biol* 2005; 170: 455–464.
42. Ito Y, Vogt PK, Hart JR. Domain analysis reveals striking functional differences between the regulatory subunits of phosphatidylinositol 3-kinase (PI3K), p85α and p85β. *Oncotarget* 2017; 8: 55863–55876.
43. Cortés I, Sánchez-Ruíz J, Zuluaga S, Calvanese V, Marqués M, Hernández C *et al*. p85β phosphoinositide 3-kinase subunit regulates tumor progression. *Proc Natl Acad Sci U S A* 2012; 109: 11318–11323.
44. Ardini E, Agresti R, Tagliabue E, Greco M, Aiello P, Yang LT *et al*. Expression of protein tyrosine phosphatase alpha (RPTPalpha) in human breast cancer correlates with low tumor grade, and inhibits tumor cell growth in vitro and in vivo. *Oncogene* 2000; 19: 4979–4987.
45. den Hertog J, Tracy S, Hunter T. Phosphorylation of receptor protein-tyrosine phosphatase alpha on Tyr789, a binding site for the SH3-SH2-SH3 adaptor protein GRB-2 in vivo. *EMBO J* 1994; 13: 3020–3032.
46. Lai X, Chen Q, Zhu C, Deng R, Zhao X, Chen C *et al*. Regulation of RPTPα-c-Src signalling pathway by miR-218. *FEBS J* 2015; 282: 2722–2734.
47. Wang J, Deng R, Cui N, Zhang H, Liu T, Dou J *et al*. Src SUMOylation Inhibits Tumor Growth Via Decreasing FAK Y925 Phosphorylation. *Neoplasia (New York, NY)* 2017; 19: 961–971.
48. Song J-W, Zhu J, Wu X-X, Tu T, Huang J-Q, Chen G-Z *et al*. GOLPH3/CKAP4 promotes metastasis and tumorigenicity by enhancing the secretion of exosomal WNT3A in non-small-cell lung cancer. *Cell Death Dis* 2021; 12: 976.
49. Jumper J, Evans R, Pritzel A, Green T, Figurnov M, Ronneberger O *et al*. Highly accurate protein structure prediction with AlphaFold. *Nature* 2021; 596: 583–589.
50. Wojdyr M. GEMMI: A library for structural biology. *Journal of Open Source Software* 2022; 7: 4200.

Figures

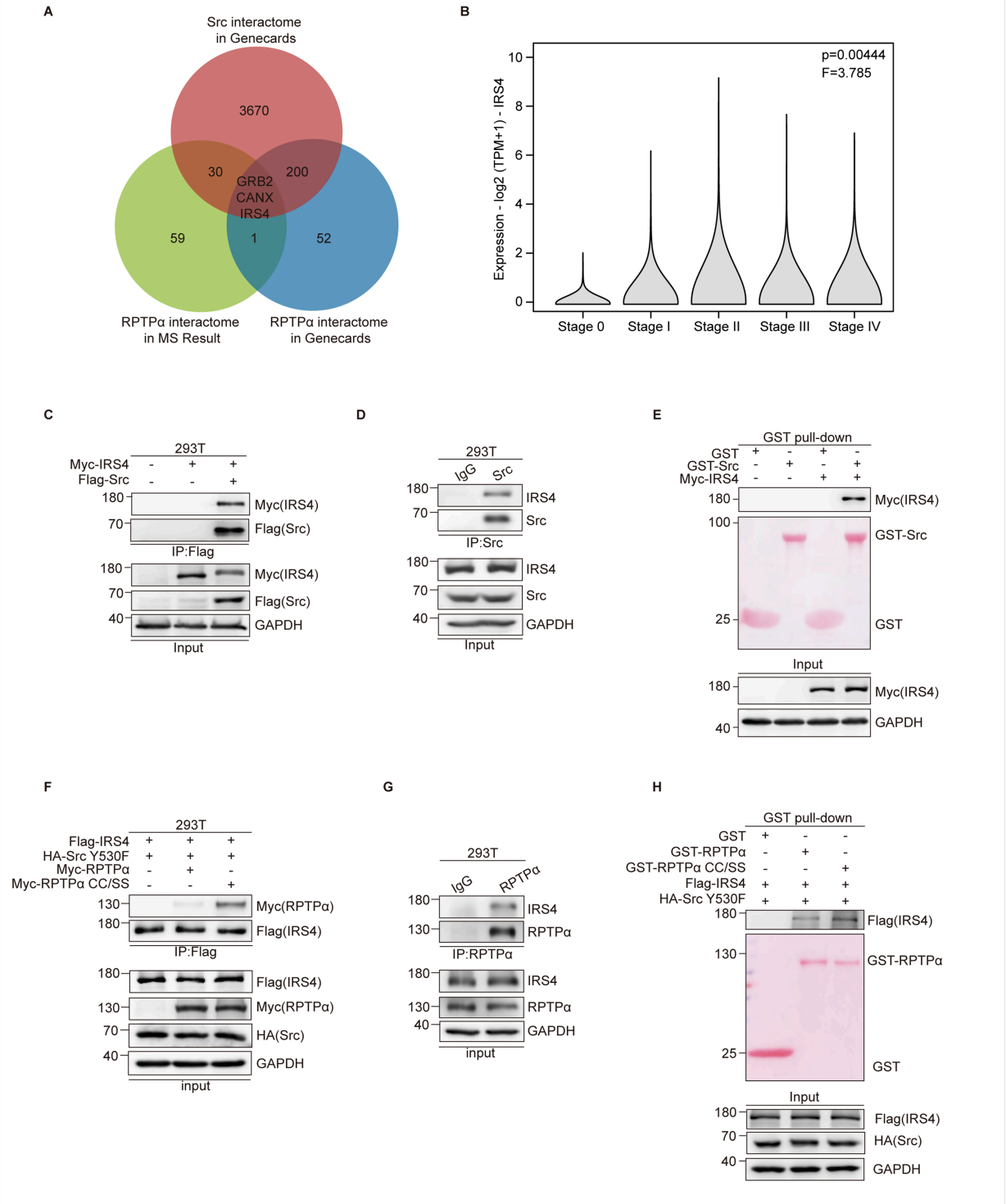

Figure 1

IRS4 interacts with both Src and RPTPα *in vivo* and *in vitro*.

(A) Venn diagram illustrating the intersection of RPTPα-interacting protein data with the predicted interactome of Src and RPTPα from the GeneCards database.

(B) Analysis of IRS4 expression across different clinical stages in 33 TCGA tumor types based on GEPIA.

(C) Co-immunoprecipitation (Co-IP) analysis in 293T cells overexpressing Myc-IRS4 and Flag-Src plasmids.

(D) Endogenous interaction analysis between native Src and IRS4 proteins in 293T cells.

(E) GST pull-down analysis demonstrating the interaction between purified GST-Src and IRS4.

(F) Co-IP analysis in 293T cells overexpressing Flag-IRS4, Myc- RPTPα-WT, or Myc- RPTPα-CC433/723SS plasmids.

(G) Endogenous interaction analysis between RPTPα and IRS4 proteins in 293T cells. (H) GST pull-down analysis showing the interaction between Flag-IRS4 and purified GST- RPTPα (WT or CC433/723SS) proteins.

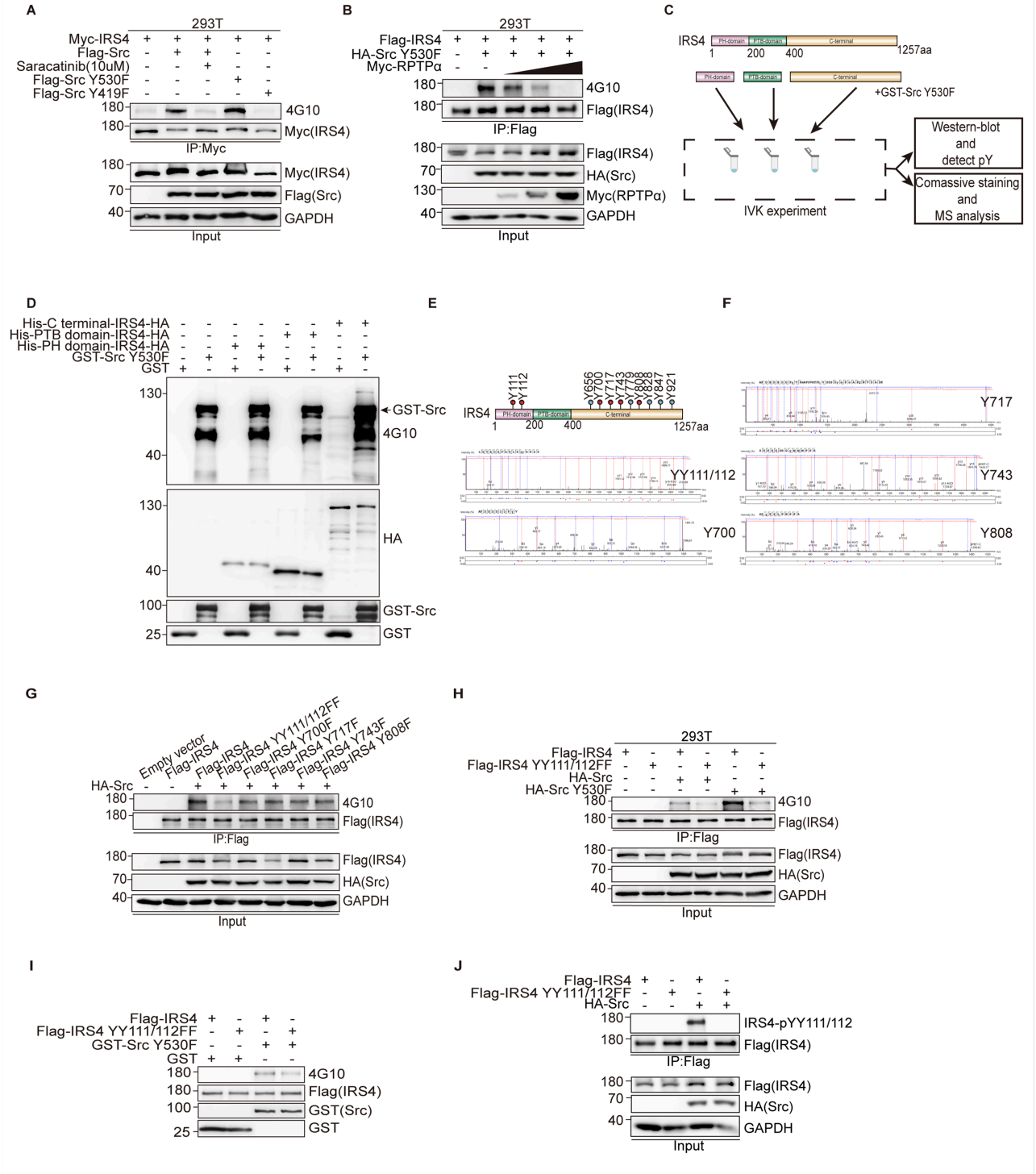

Figure 2

Phosphosite analysis of IRS4 by Src.

(A)293T cells were co-transfected with Myc-IRS4 and Flag-Src (WT, kinase-activated Y530F, or kinase-dead Y419F), with or without Saracatinib (10 μM). IRS4 was immunoprecipitated with anti-Myc and analyzed by WB.

(B) RPTPα dephosphorylates IRS4 in a dose-dependent manner. 293T cells were co-transfected with Myc-IRS4 and active Flag-Src (Y530F), together with increasing amounts of RPTPα, followed by WB analysis.

(C) Schematic of IRS4 domain structure and the design of the *in vitro* kinase assay using purified IRS4 truncation mutants.

(D) *In vitro* kinase assay showing Src-mediated phosphorylation of IRS4 domains. Purified His-tagged IRS4 truncations were incubated with GST-Src Y530F and analyzed by WB.

(E, F) Identification of Src-induced IRS4 phosphorylation sites by mass spectrometry. (G) 293T cells were co-transfected with HA-Src and Flag-tagged IRS4-WT or the indicated Y-to-F mutants. IRS4 was immunoprecipitated with anti-Flag and tyrosine phosphorylation was detected by 4G10 IB.

(H) 293T cells were transfected with Flag-IRS4-WT or Flag-IRS4-YY111/112FF together with HA-Src or HA-Src Y530F, followed by WB analysis.

(I) *In vitro* kinase assay using purified GST-Src and Flag- IRS4-WT or Flag-IRS4-YY111/112FF. Proteins were incubated with ATP-containing kinase buffer for 1h and analyzed by WB.

(J) Validation of the phosphosite-specific IRS4 pYY111/112 antibody in 293T cells expressing Flag-IRS4-WT or IRS4-YY111/112FF, with or without HA-Src.

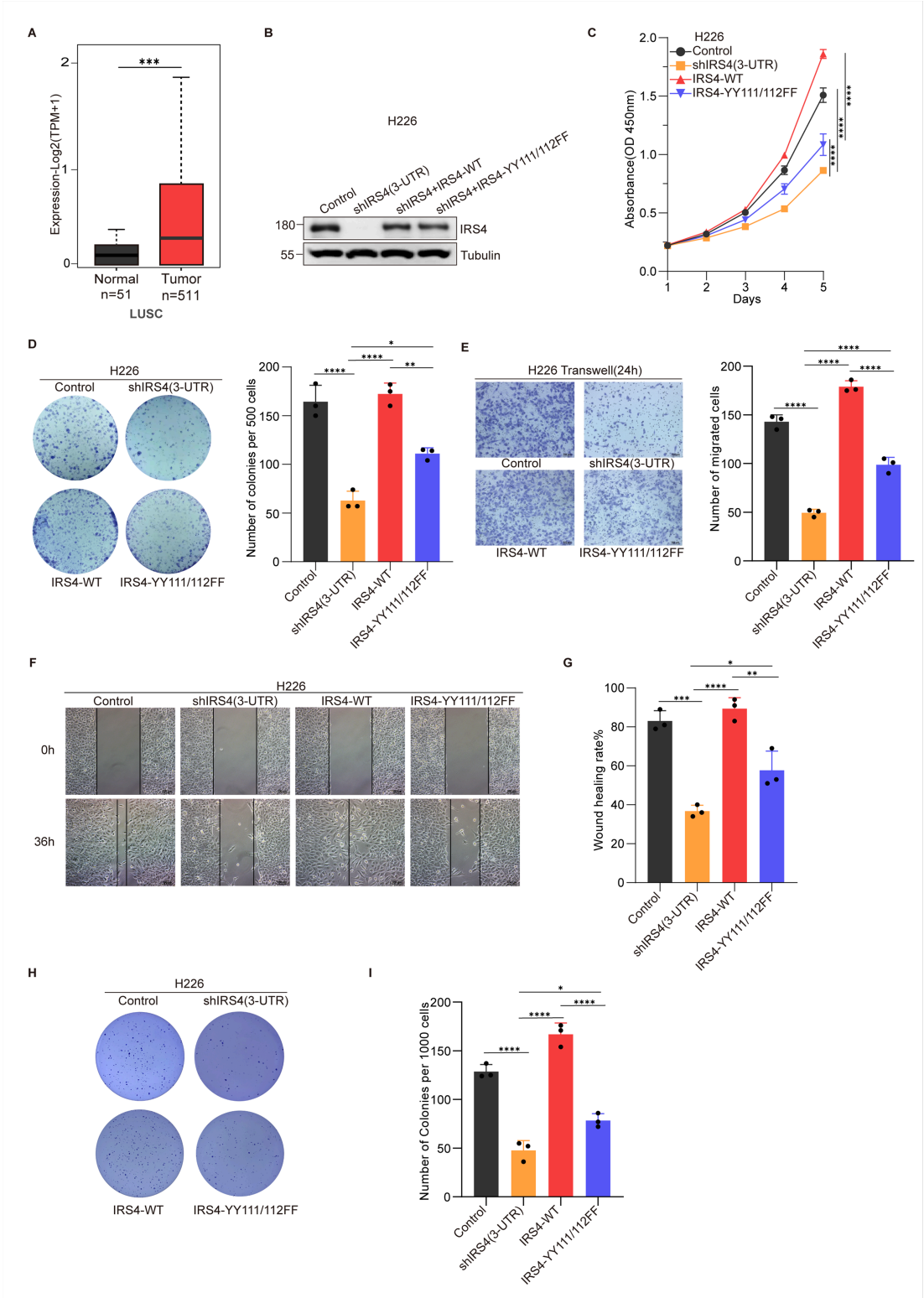

Figure 3

Tyrosine phosphorylation of IRS4 at YY111/112 is essential for its oncogenic functions in LUSC cells.

(A) mRNA expression analysis of *IRS4* in Lung Squamous Cell Carcinoma (LUSC) tissues (n=486) and adjacent normal tissues (n=338) using the TCGA database. Data are shown as log_2(TPM+1).

(B) Western blot analysis of IRS4 expression in H226, H226 ^{shIRS4}, H226 ^{shIRS4}-IRS4-WT, H226 ^{shIRS4}-IRS4-YY111/112FF stable cell lines.

(C) CCK-8 assays were used to detect the cell viability of H226, H226 ^{shIRS4}, H226 ^{shIRS4}-IRS4-WT, H226^{shIRS4}-IRS4-YY111/112FF stable cell lines for 5 d (n =4).

(D) Colony formation assays were used to evaluate the colony-forming ability of H226, H226 ^{shIRS4}, H226^{shIRS4}-IRS4-WT, H226^{shIRS4}-IRS4-YY111/112FF stable cell lines (n =3).

(E) Transwell migration assay was used to evaluate the migration ability of H226, H226 ^{shIRS4}, H226^{shIRS4}-IRS4-WT, or H226 ^{shIRS4}-IRS4-YY111/112FF stable cell lines after 24 h post-seeding (n =3).

(F, G) Wound healing assay was conducted to assess the migration ability of H226, H226 ^{shIRS4}, H226^{shIRS4}-IRS4-WT, or H226^{shIRS4}-IRS4-YY111/112FF stable cell lines after 48 h post-seeding (n =3).

(H, I) Soft-agar colony formation assay used to evaluate anchorage-independent growth of H226, H226^{shIRS4}, H226^{shIRS4}-IRS4-WT, or H226^{shIRS4}-IRS4-YY111/112FF stable cell lines and quantification (n =3). Statistical analysis was performed using one-way ANOVA or two-way ANOVA with multiple comparisons. *P < 0.05; **P < 0.01; ***P < 0.001; ****P < 0.0001. ; ns, not significant.

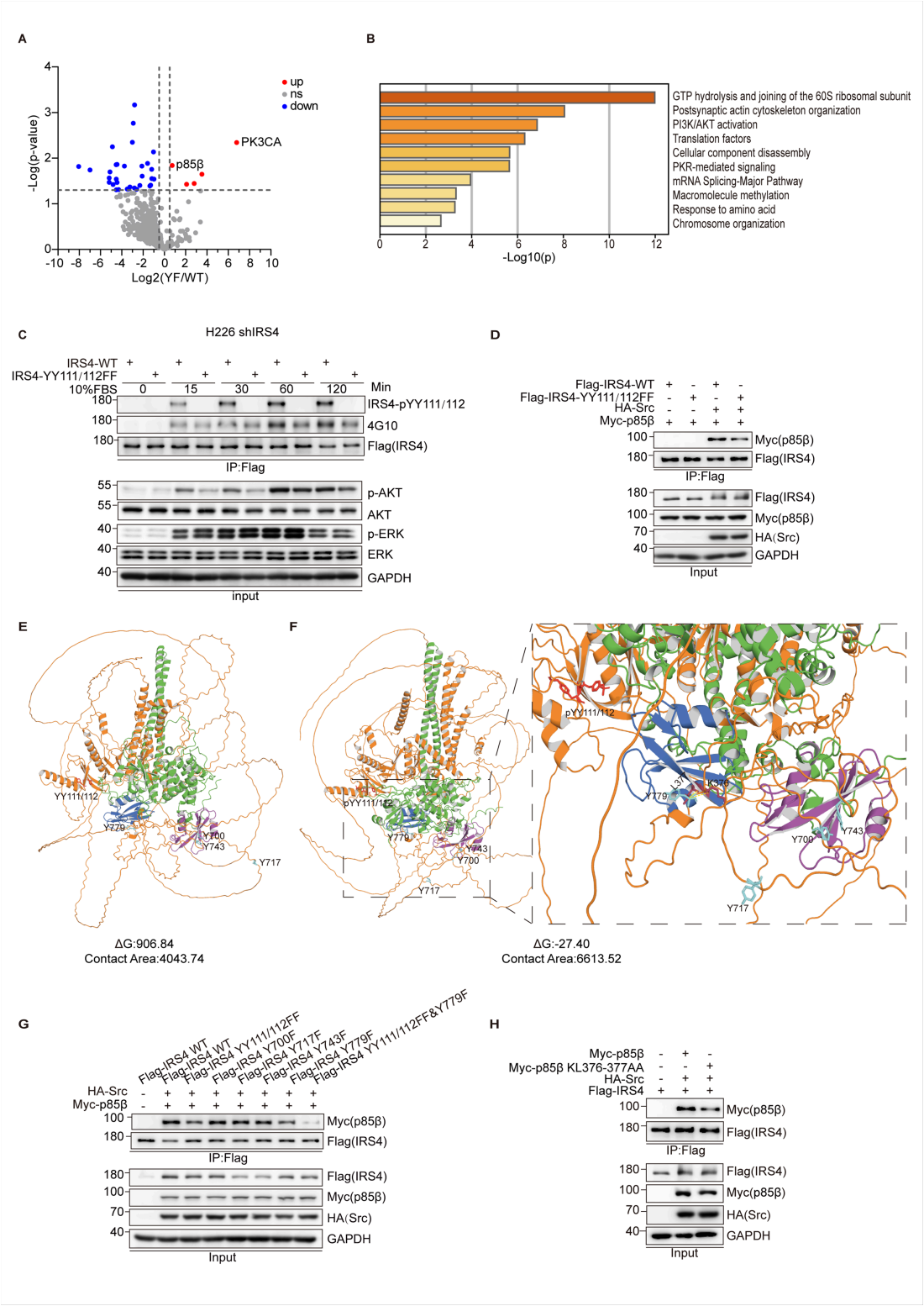

Figure 4

Phosphorylation of IRS4 at YY111/112 promotes p85β recruitment and activates PI3K–AKT signaling

(A) Volcano plot displaying differentially enriched proteins identified by immunoprecipitation–mass spectrometry (IP-MS) comparing IRS4-WT and IRS4-YY111/112FF mutants. Proteins significantly upregulated (up), downregulated (down), or no significant (ns) are indicated.

(B) Gene Ontology (GO) and pathway enrichment analysis of the differential data from (A).

(C) H226^{shIRS4}-IRS4-WT, or H226^{shIRS4}-IRS4-YY111/112FF stable cell lines were stimulated with 10% FBS for the indicated time points. Followed by IP and WB to analyze IRS4 phosphorylation and downstream AKT/ERK signaling.

(D) 293T cells co-transfected with HA-Src, Myc-p85β, and Flag-IRS4-WT or Flag-IRS4-YY111/112FF. Co-IP analyzed the interaction between IRS4 and p85β.

(E) AlphaFold-predicted structural models of the IRS4-p85β complex in the unphosphorylated state.

(F) AlphaFold-predicted structural models analysis of the IRS4 and p85β complex in the phosphorylated state.

(G) 293T cells were transfected with Flag-IRS4-WT or various Flag-IRS4 mutants along with HA-Src and Myc-p85β, analyzed by Co-IP.

(H) 293T cells were transfected with Flag-IRS4, Myc-p85β, or Myc-p85β-KL376-377AA in the presence of HA-Src, analyzed by Co-IP.

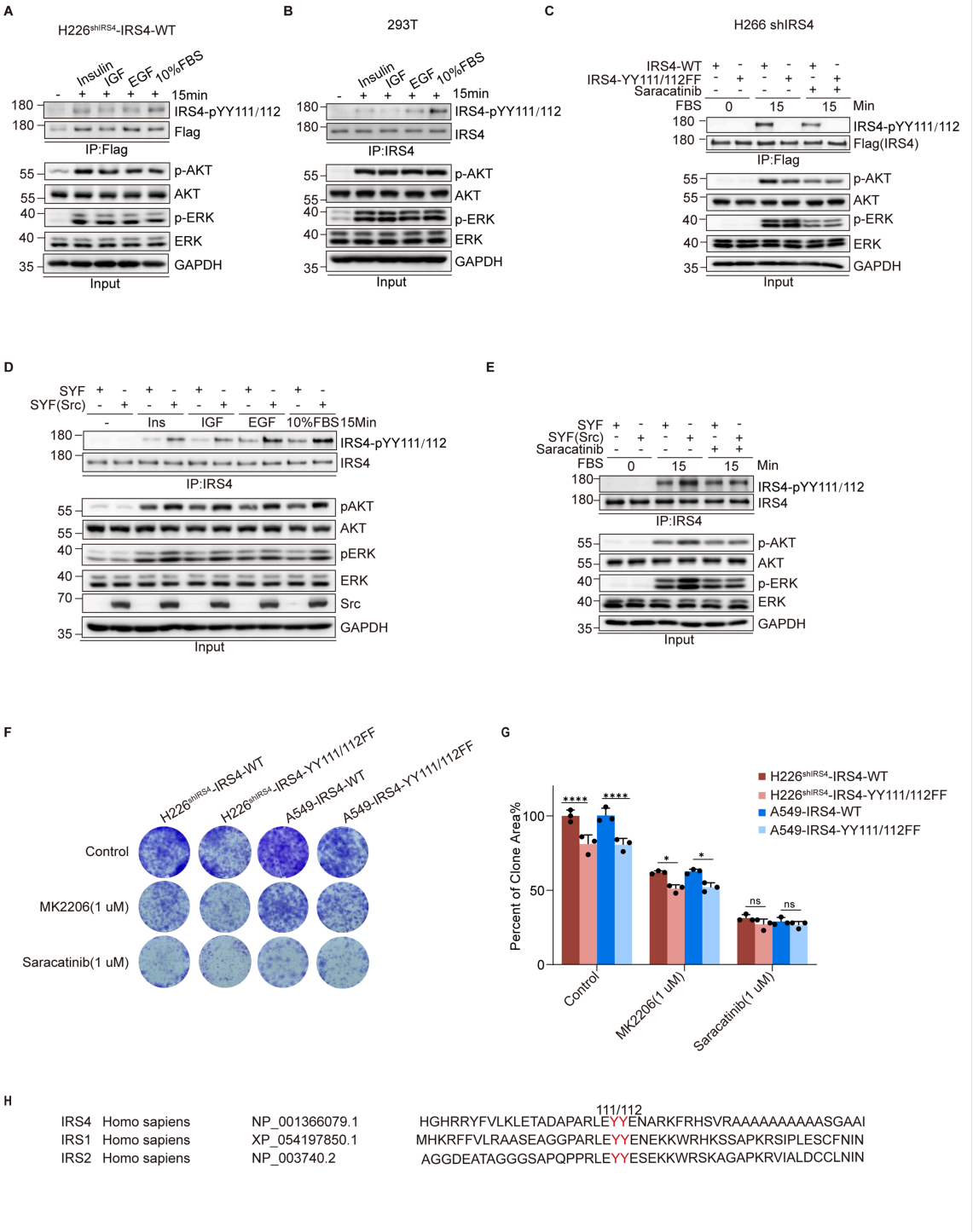

Figure 5

Various growth factor stimulations cause phosphorylation of the Y111/112 site.

(A) H226^{shIRS4}-IRS4-WT cells were serum-starved and stimulated with Insulin (200 mM), IGF (50 ng/mL), EGF (50 ug/mL), or 10 % FBS for 15 min. Cell lysates were subjected to IP and WB.

(B) Serum-starved 293T cells were stimulated with insulin, IGF, EGF, or 10% FBS, followed by IP and WB.

(C) H226^{shIRS4}-IRS4-WT, or H226^{shIRS4}-IRS4-YY111/112FF cells were treated with or without the Src inhibitor Saracatinib (10 μM) for 4 h before being stimulated with 10 % FBS as indicated. Cell lysates were subjected to IP and WB.

(D) SYF or SYF-Src cells were serum-starved and stimulated with insulin, IGF, EGF, or 10% FBS for 15 min, followed by IP and WB.

(E) SYF or SYF-Src cells were treated with or without Saracatinib (10 μM) before 10% FBS stimulation, followed by IP and WB.

(F) Representative images of colony formation assays in H226^{shIRS4}-IRS4-WT, or H226^{shIRS4}-IRS4-YY111/112FF cells, and A549-IRS4-WT, or A549-IRS4-YY111/112FF cells, treated with MK2206 (1 μM), or Saracatinib (1 μM).

(G) Quantification of colony area in (F).

(H) Sequence alignment of human IRS family members showing conservation of IRS4 YY111/112 site. Data are presented as a percentage of the clone area relative to the control. Data represent mean ± SD from three independent experiments. Two-tailed Student's t-test determined statistical significance. *P < 0.05; **P < 0.01; ***P < 0.001; ****P < 0.0001; ns, not significant.

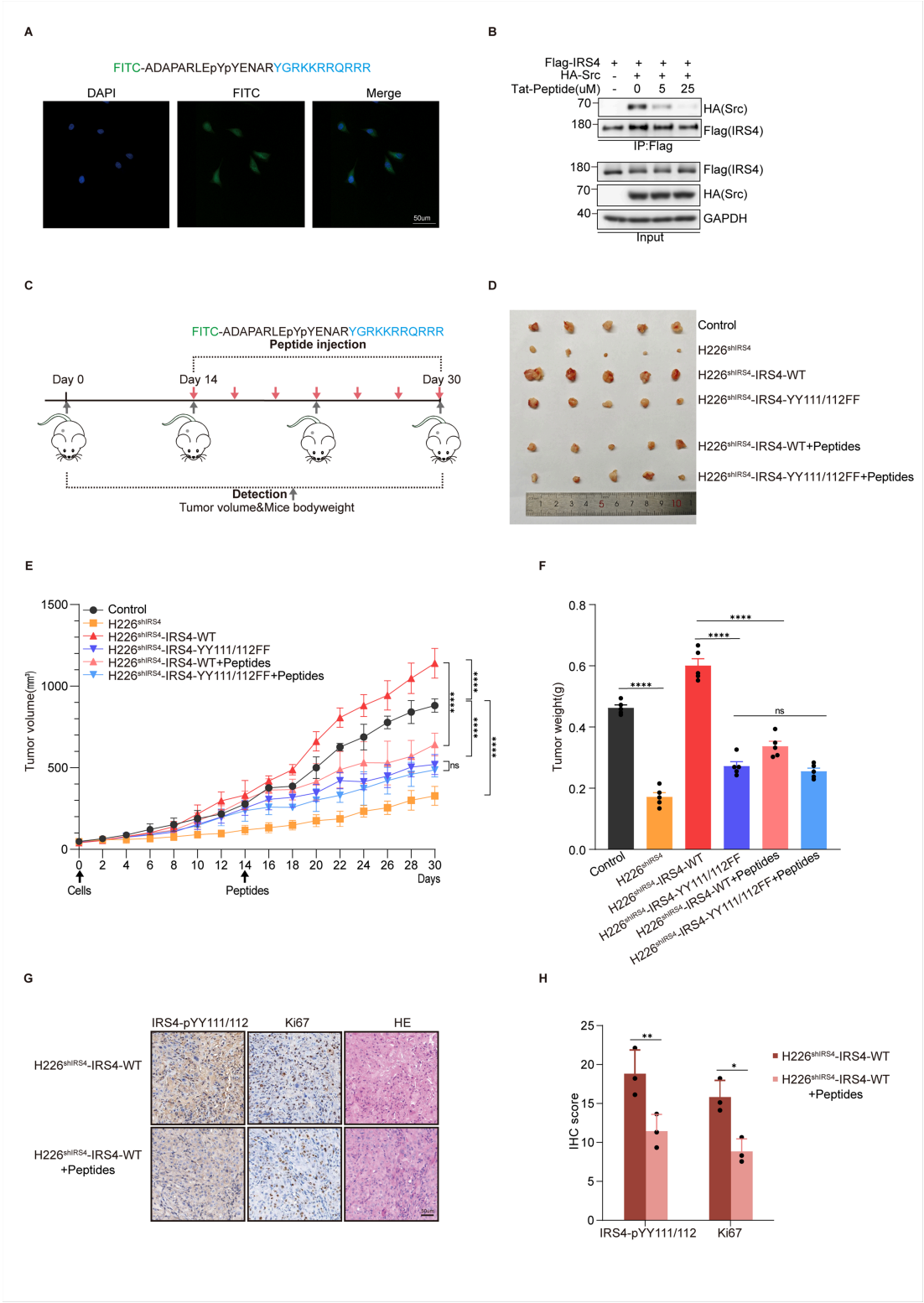

Figure 6

pYY111/112 peptide blocks IRS4-Src interaction and suppresses tumor growth.

(A) Cellular uptake of FITC-labeled Tat-coupled phosphopeptides. H226 cells were incubated with the FITC-ADAPARLEpYpYENARYGRKKRRQRRR peptide, and representative fluorescence images are shown. Scale bar: 50 μm.

(B)293T cells co-transfected with Flag-IRS4, Myc-p85β, and HA-Src were treated with the indicated Tat-peptide, followed by Flag-IP and immunoblotting to assess the IRS4–Src interaction.

(C) Schematic of the xenograft experiment. H226 stable cells were subcutaneously injected into nude mice, and Tat-peptide treatment was initiated on day 14. Tumor volume and body weight were monitored every 2 days until day 30.

(D) Representative images of excised tumors at the endpoint.

(E) Tumor growth curves of H226 xenografts in the indicated groups. Data are shown as mean ± SD (*n* = 5).

(F) Tumor weights at the endpoint. Data are shown as mean ± SD (*n* = 5).

(G) IHC staining of xenograft sections for pYY111/112, Ki67, or H&E. Representative images are shown. Scale bar, 50 μm.

(H) Quantification of IHC intensity and Ki67-positive cells. Data are presented as mean ± SD. Statistical significance was determined by one-way ANOVA or two-way ANOVA. *P < 0.05; **P < 0.01; ***P < 0.001; ****P < 0.0001. ; ns, not significant.

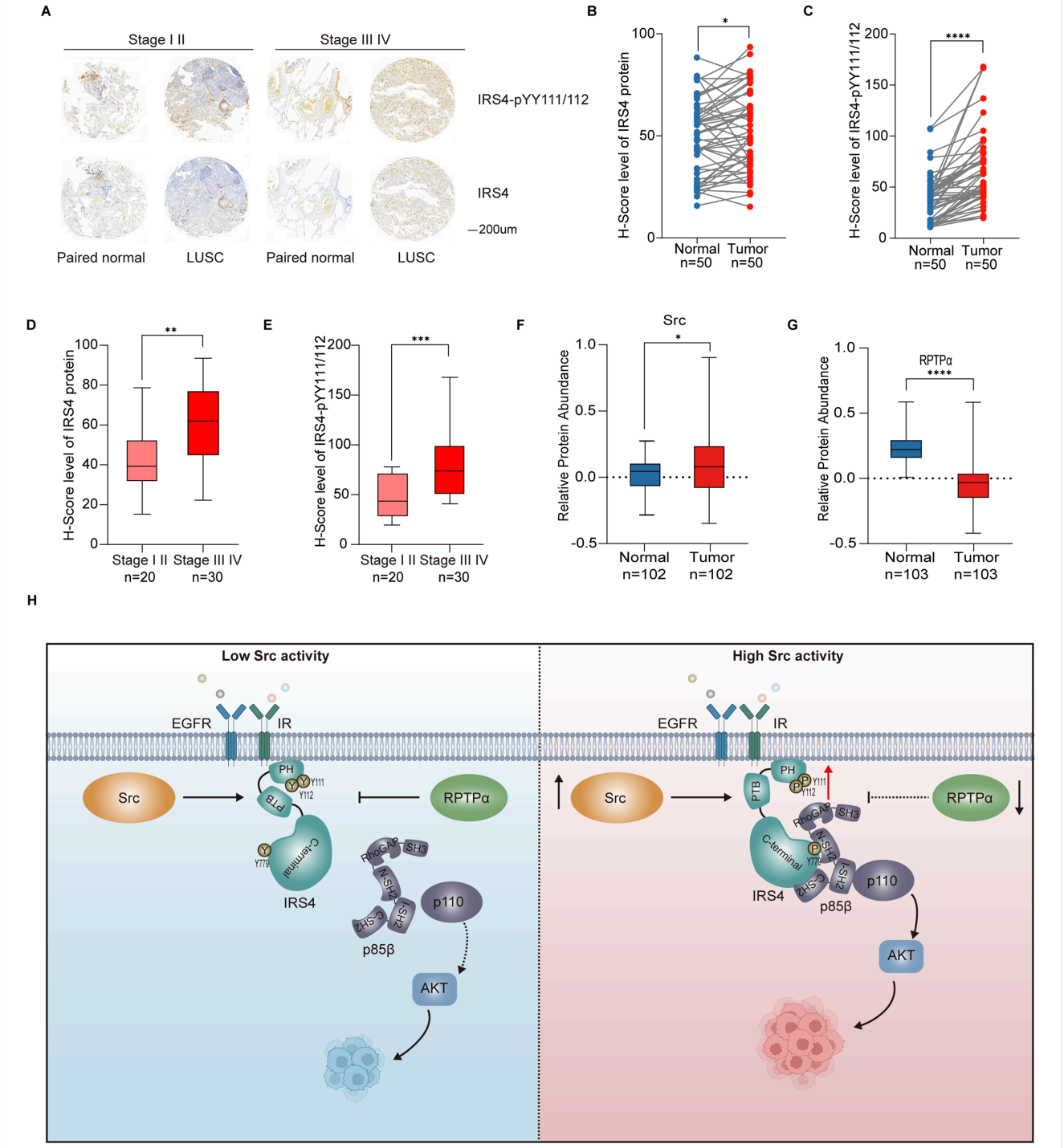

Figure 7

YY111/112 phosphorylation is upregulated and positively correlated with human LUSC progression.

(A) Representative IHC staining of pYY111/112 and IRS4 in paired normal lung tissues and LUSC samples from stage I–II and stage III–IV patients. Scale bar, 200 μm.

(B) Paired analysis of H-scores for IRS4 in matched normal lung tissues and LUSC tumors (n = 50 pairs).

(C) Paired analysis of H-scores for pYY111/112 in matched normal lung tissues and LUSC tumors (*n* = 50 pairs).

(D) Comparison of IRS4 H-scores between early-stage (I–II, n = 20) and advanced-stage (III–IV, n=30) LUSC samples.

(E) Comparison of pYY111/112 H-scores between early-stage (I–II, n = 20) and advanced-stage (III–IV, n=30) LUSC samples.

(F) Relative protein abundance of Src in normal lung tissues and LUSC tumors based on CPTAC proteomic data.

(G) Relative protein abundance of RPTPα in normal lung tissues and LUSC tumors based on CPTAC proteomic data.

(H) Proposed model illustrating that Src-mediated phosphorylation of IRS4 at YY111/112 promotes p85β recruitment and AKT activation, whereas RPTPα opposes this process by dephosphorylating the same site. Increased Src activity disrupts this regulatory balance, leading to sustained IRS4 YY111/112 phosphorylation and consequent promotion of LUSC progression.

Statistical significance was assessed using the Wilcoxon matched-pairs signed-rank test for A and B. Statistical significance was determined using a paired two-tailed Student's *t*-test, as appropriate. (*P < 0.05; **P < 0.01; ***P < 0.001; ****P < 0.0001; ns, not significant.)

Supplementary Files

This is a list of supplementary files associated with this preprint. Click to download.

- TableS1.docx
- Supplementaryfigurelegends.docx
- Fig.S3.tif
- Fig.S4.tif
- Fig.S5.tif
- Fig.S2.tif
- Fig.S1.tif
- Fig.S6.tif